Journal of Sound and Vibration 339 (2015) 84–98

Contents lists available at ScienceDirect

Journal of Sound and Vibration

journal homepage: www.elsevier.com/locate/jsvi

Relieving the effect of static load errors in nonlinear vibration isolation mounts through stiffness asymmetries

A.D. Shaw [a,*], S.A. Neild [b], M.I. Friswell [a]

[a] College of Engineering, Swansea University, Swansea SA2 8PP, United Kingdom
[b] Department of Mechanical Engineering, University of Bristol, Queen's Building, Bristol BS8 1TR, United Kingdom

ARTICLE INFO

Article history:
Received 30 May 2014
Received in revised form
17 September 2014
Accepted 3 November 2014
Handling Editor: M.P. Cartmell
Available online 24 November 2014

ABSTRACT

High Static Low Dynamic Stiffness (HSLDS) mounts consist of nonlinear springs that support a high static load with low static displacement, whilst maintaining locally low stiffness near equilibrium, to give a low natural frequency and consequently good isolation properties. Recent analysis has investigated such devices when the force–displacement relationship is an odd function about the equilibrium position, and analysed the consequences of different shapes of these functions. However many devices that have the HSLDS characteristic do not meet the assumptions of this analysis, in that the force–displacement relationship is generally asymmetric about equilibrium. Furthermore, even devices that do meet this assumption may be subject to significant adjustment error, particularly in the context of air vehicles where manoeuvres such as banked turns can cause an apparent variation in gravitational acceleration, and a consequent variation in the weight of the payload. This change in static load moves the payload away from its intended region of low stiffness. The current paper provides analysis of these situations, and shows that the performance of a mount with a symmetric stiffness–displacement relationship is highly sensitive to errors in the static loading. It is then shown that a mount with an asymmetric stiffness–displacement function can offer significant performance advantages when there are adjustment errors in the loading of the mount.

1. Introduction

Vibration isolation is a vital requirement throughout much of engineering [1], particularly when there is a strong source of vibration such as a motor. It is frequently required to prevent the transmission of these vibrations to other elements of the system, for reasons such as passenger comfort in vehicles, or the protection of delicate electronic equipment. A typical means of protecting equipment from a source of vibration is by placing it upon a vibration isolation mount.

A High Static Low Dynamic Stiffness (HSLDS) mount is a vibration isolation mount based on a nonlinear spring, that means that near the static equilibrium point stiffness is low, whilst elsewhere stiffness increases to ensure that deflections due to static load bearing remain acceptable [2]. The low dynamic stiffness means that near resonance the frequency at which the peak response occurs, ω_0, is low. In the case of base excitation, as is considered in this work, the peak amplitude

* Corresponding author.
E-mail address: a.d.shaw@swansea.ac.uk (A.D. Shaw).

http://dx.doi.org/10.1016/j.jsv.2014.11.006
0022-460X/

will also be low. The low dynamic stiffness also benefits the isolation region, by giving a low isolation frequency, which is the frequency above which the transmissibility is less than unity (for a linear system the isolation frequency is given by $\omega_i = \sqrt{2k/m}$ [2]). A low isolation frequency means that a larger frequency band experiences isolation, and leads to reduced transmissibility up until very high frequencies where transmissibility is dominated by damping. The High Static Low Dynamic Stiffness (HSLDS) mount can achieve these benefits whilst maintaining good static stiffness for load bearing, whereas for linear mounts the stiffness must be chosen as a direct trade off between static and dynamic concerns.

1.1. Prior work on HSLDS isolation mounts

Numerous isolators that exhibit HSLDS behaviour have appeared in the literature, although the HSLDS term itself is relatively new. Winterflood [3] presents a mount utilising a Euler spring for use in gravitational experiments. Virgin and Davis [4] present a prototype mount consisting of a buckled strut, and Plaut et al. [5] present analysis of a similar mount albeit with fixed as opposed to pinned end conditions. Virgin et al. [6] also propose a mechanism based on a strip bent into a tear-shaped loop. Further results for both these types of mount appear in Santillan's PhD thesis [7]. DeSalvo [8] presents a general design deriving the required nonlinear response from a geometrical arrangement of springs, and presents results from an implementation using prestressed blade springs. Carrella et al. [9] present analysis of a similar geometrical spring arrangement, with the aim of achieving near zero stiffness at equilibrium, known as Quasi-Zero Stiffness (QZS). In a more recent paper, Carrella et al. idealised the dynamic response of this mechanism as a Duffing oscillator, demonstrating important differences between its force transmissibility and motion transmissibility [10]. Kovacic et al. [11] also proposed oblique spring arrangements, but with nonlinear springs to reduce the variability in dynamic stiffness with displacement from equilibrium. Zhou and Liu have proposed an HSLDS using an electromagnetic negative spring element that allows system parameters to be tuned [12]. Robertson et al. [13] present theoretical analysis for a fully magnetic HSLDS device, where magnetism also supports the payload mass. Many HSLDS devices are included in a review of passive vibration isolation methods by Ibrahim [14]. Further designs, both magnetic and geometric, and more analysis of the nonlinear phenomena encountered by HSLDS mounts including amplitude dependent response and jump frequencies, based on Duffing oscillator models, are given in [2]. In addition, Le and Ahn present analysis and an experimental prototype for a spring-based mechanism designed for isolation of a vehicle seat [15], showing that isolation is achieved for both broadband and harmonic signals. Recently, Xu et al. produced a successful experiment that demonstrated the HSLDS concept when used to minimise force transmissibility [16].

Huang et al. created an experimental isolator exploiting negative stiffness from an arrangement of buckled beams [17]. This work appears to be the first that makes detailed consideration of the effects of adjustment errors on a nonlinear spring isolator. It shows that imperfections in the load can change the nature of the low amplitude response of the mass–spring system from a hardening system to a softening system. Huang et al. extend the theoretical conclusions of this work in [18,19], showing that having a very low minimum mount stiffness is not necessarily conducive to the best isolation in the presence of stiffness or loading errors.

A High Static Low Dynamic Stiffness (HSLDS) mount is a vibration isolation mount based on a nonlinear spring, that means that near the static equilibrium point stiffness is low, whilst elsewhere stiffness increases to ensure that deflections due to static load bearing remain acceptable [2]. The low dynamic stiffness means that in the resonant region of frequency response the frequency of peak response ω_0 is low, and in the case of base excitation considered in this work, the peak amplitude will be low as well. It also benefits the isolation region, by giving a low isolation frequency, which is the frequency above which the transmissibility is less than unity (for a linear system the isolation frequency is given by $\omega_i = \sqrt{2k/m}$ [2]). A low isolation frequency means that more frequencies experience isolation, and leads to reduced transmissibility up until very high frequencies where transmissibility is dominated by damping. The High Static Low Dynamic Stiffness (HSLDS) mount can achieve these benefits whilst maintaining good static stiffness for load bearing, whereas for linear mounts the stiffness must be chosen as a direct trade off between static and dynamic concerns.

1.2. Overview of the current work

The discussion in Section 1.1 highlights the diversity in the physical implementations of HSLDS mounts that have been studied, and this diversity has led to a wide variety in the shape and mathematical forms of the force–displacement curves for the nonlinear springs created. However in the vast majority of analyses, the springs have been idealised with Duffing or even linear approximations, masking many differences between the various force–displacement functions used. In order to begin answering the question of which shape for the force displacement curve was most desirable from a dynamical point of view, the authors recently provided a higher order dynamic analysis of the HSLDS concept [20]. This work used a fifth-order polynomial function for force displacement instead of the more usual third-order model, and showed that subtle changes to the force–displacement curve of the spring could have drastic effects upon the dynamic response.

The work presented here extends the analysis of [20], by relaxing the assumption that the mount has a symmetric stiffness–displacement response. Firstly, this allows the analysis to be applied to a wider range of devices, such as those considered by Winterflood [3] and Virgin [4]. Secondly, it naturally leads to consideration of the effect of errors in the static load on the isolation performance of the mount; HSLDS mounts depend on operating about a specified static equilibrium point, and it is shown that they are therefore highly sensitive to errors in the static load. Effects similar to those found in

[17–19] are found, and studied in detail, and are shown to cause a limitation on the amount by which the dynamic stiffness may be reduced. The form of error considered is that of an additional constant acceleration term expressed as an apparent change in gravity, as may be experienced in an aircraft during a banked turn. Other forms of error such as changes in the payload mass or loss of adjustment in the mechanism are not considered, but the analysis provided could easily and intuitively be adapted for this purpose.

It is shown that an HSLDS mount designed to have an extremely low dynamic stiffness, known as a Quasi-Zero Stiffness (QZS) mount, will be highly sensitive to loading errors, and that a more moderately reduced stiffness mount will often give better performance under realistic operating conditions. Furthermore, it is shown that mounts with asymmetric stiffness may offer moderately better performance than ones with symmetric stiffness under ideal conditions. Furthermore, they may also give substantially improved performance if the sign of the loading error can be anticipated.

2. Analysis

2.1. Idealisation and nondimensionalisation of system

Fig. 1 illustrates the idealised system under consideration. Mass m is supported above a base by a nonlinear spring with a force–displacement curve given by $P_k(z)=P(z)+F_s$, where $z\equiv x-r$ is the relative displacement of the mass, x is the absolute displacement of the mass and r is the displacement of the base. F_s is the static force that the mount supports; typically this is equal to the weight of the mass i.e. mg and this is assumed to be the case in this analysis. The static displacement is denoted z_s, and is the magnitude of displacement that the mount encounters on the application of the static load F_s. It is also natural to define $k_s\equiv F_s/z_s$ as the static stiffness of the system; this is the stiffness of an equivalent linear system that has the same static load and static displacement.

Using free body diagram analysis, the equation of motion of this system can be determined as

$$m\ddot{z}+c\dot{z}+P(z)=-\ddot{r}m \tag{1}$$

F_s and z_s are fundamental requirements for the static load bearing performance of the mount; it must support the static load without exceeding a maximum value for static displacement. Therefore F_s and z_s are used to nondimensionalise forces and displacements respectively:

$$\hat{x}=\frac{x}{z_s},\quad \hat{r}=\frac{r}{z_s},\quad \hat{z}=\frac{z}{z_s},\quad \hat{P}(\hat{z})=\frac{P(z_s\hat{z})}{F_s} \tag{2}$$

Furthermore, time is nondimensionalised as

$$\tau=t\omega_s \tag{3}$$

where $\omega_s\equiv\sqrt{k_s/m}$ is the natural frequency of the equivalent linear system with equal static force and displacement. The damping ratio of this system is also employed, defined as

$$\lambda=\frac{c}{\sqrt{2mk_s}} \tag{4}$$

All nondimensional terms are substituted into Eq. (1) to give

$$\hat{z}''+2\lambda\hat{z}'+\hat{P}(\hat{z})=-\hat{r}'' \tag{5}$$

where $'$ indicates differentiation with regard to τ.

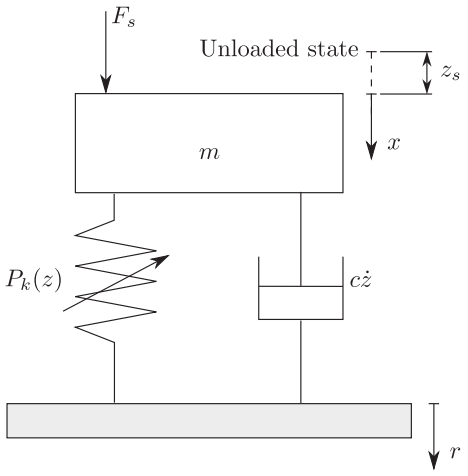

Fig. 1. Idealisation of mass m supported by nonlinear spring and damper above base. The unloaded state indicates the position of the mass when F_s is not applied.

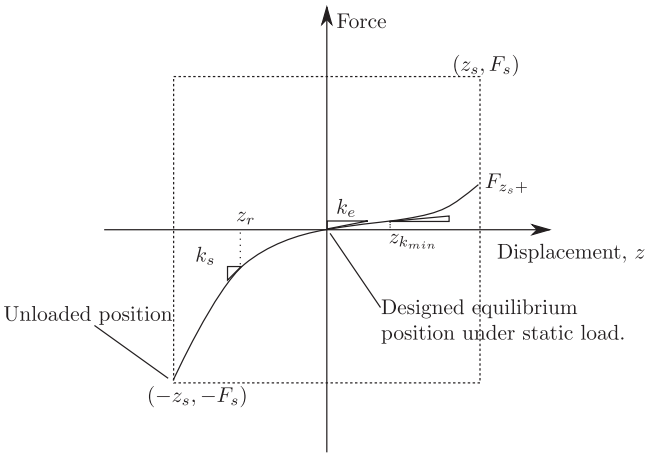

Fig. 2. Shape properties of an asymmetric HSLDS force displacement curve.

2.2. Shape properties of HSLDS force–displacement relationship

While a polynomial representation of the force displacement curve allows a wide range of possible responses and facilitates analysis, it is hard to gain physical intuition of the effects of varying individual polynomial coefficients. Therefore, the force–displacement curve is discussed in terms of four nonlinear shape properties that allow greater intuition.

Fig. 2 illustrates the shape properties on an arbitrary asymmetric HSLDS force–displacement curve. It is assumed that the static force and displacement occur in a positive direction when applied to the mass and that therefore the unloaded state is at $(-z_s, -F_s)$.

The first two shape properties, k_e and z_r, are as defined previously in [20] but recapped here. The stiffness at static equilibrium is naturally referred to as the equilibrium stiffness k_e, and maybe considered to be the dynamic stiffness for small oscillation about equilibrium. The response is designed so that $k_e < k_s$, to achieve a low natural frequency. The parameter z_r is known as the reduced stiffness range, and is the displacement towards the unloaded state over which the stiffness of the nonlinear response is less than that of the equivalent linear stiffness.

In this document, two further parameters are introduced which extend the work in [20] by introducing asymmetry to the stiffness–displacement response. The first of these is the positive static displacement force F_{z_s+}, which is the restoring force encountered at a displacement of z_s beyond the designed equilibrium position. This parameter allows modelling of asymmetric mounts such as the postbuckled beams described by Virgin [4], which have high stiffness near the unloaded condition, but not at displacements beyond their designed equilibrium positions. For symmetric systems, $F_{z_s+} = F_s$; in general $F_{z_s+} < F_s$ as the majority of anti-vibration mounts experience static loading in one direction only, and there is no need to locate high stiffness where there is no advantage to static load bearing. The second parameter is the displacement at minimum stiffness, $z_{k_{min}}$, which relaxes the assumption in [20] that the minimum stiffness is located at the static equilibrium point. Changes to these parameters can lead to performance advantages in the case of static loading errors, as shall be demonstrated in Section 3.3.

2.3. Resolving nondimensional polynomial coefficients from chosen shape parameters

Nondimensional shape properties are defined by scaling using the static force and static displacement as before, hence

$$\hat{z} = \frac{z_r}{z_s}, \quad \hat{k}_e = \frac{k_e}{k_s}, \quad \hat{z}_{k_{min}} = \frac{z_{k_{min}}}{z_s}, \quad \hat{F}_{zs+} = \frac{F_{zs+}}{F_s} \tag{6}$$

It is to be noted that in the nondimensional scheme, the static force, static displacement and static stiffness all have magnitudes of 1.

A fifth-order polynomial model is used for the form of $\hat{P}(\hat{z})$, in order to allow sufficient constants for all geometric properties to be uniquely matched, hence

$$\hat{P}(\hat{z}) = k_1\hat{z} + k_2\hat{z}^2 + k_3\hat{z}^3 + k_4\hat{z}^4 + k_5\hat{z}^5 \tag{7}$$

In order to match the force displacement shown in Fig. 2, the following mathematical conditions must be met. Firstly, to obtain the condition of static force at static displacement we give

$$\hat{P}(-1) = -1 \tag{8}$$

To obtain the static stiffness at the reduced stiffness range we give

$$\left.\frac{\mathrm{d}\hat{P}}{\mathrm{d}\hat{z}}\right|_{-\hat{z}_r} = 1 \tag{9}$$

To obtain the equilibrium stiffness we give

$$\left.\frac{\mathrm{d}\hat{P}}{\mathrm{d}\hat{z}}\right|_{0} = \hat{k}_e \tag{10}$$

Locating minimum stiffness at $\hat{z} = \hat{z}_{k_{\min}}$ implies that

$$\left.\frac{\mathrm{d}^2\hat{P}}{\mathrm{d}\hat{z}^2}\right|_{\hat{z}_{k_{\min}}} = 0 \tag{11}$$

Finally matching the positive static displacement force gives

$$\hat{P}(1) = \hat{F}_{z_s+} \tag{12}$$

Combining Eqs. (7)–(12) gives a system of linear equations in $k_1 \ldots k_5$ expressed in matrix form as

$$\begin{bmatrix} -1 & 1 & -1 & 1 & -1 \\ 1 & -2\hat{z}_r & 3\hat{z}_r^2 & -4\hat{z}_r^3 & 5\hat{z}_r^4 \\ 1 & 0 & 0 & 0 & 0 \\ 0 & 2 & 6\hat{z}_{k_{\min}} & 12\hat{z}_{k_{\min}}^2 & 20\hat{z}_{k_{\min}}^3 \\ 1 & 1 & 1 & 1 & 1 \end{bmatrix} \begin{bmatrix} k_1 \\ k_2 \\ k_3 \\ k_4 \\ k_5 \end{bmatrix} = \begin{bmatrix} -1 \\ 1 \\ \hat{k}_e \\ 0 \\ \hat{F}_{z_s+} \end{bmatrix} \tag{13}$$

Hence it is possible to set the polynomial coefficients to give the desired shape properties of the force displacement. Note that some combinations of shape parameters may result in unexpected shapes of the force–displacement curve, because the fifth-order polynomial has up to 4 turning points, some of which may be located within the region of interest (see [20] for more discussion of this issue). Therefore force–displacement plots must be checked to ensure that the parameters chosen give a sensible curve shape before dynamic analysis is conducted. This can usually be performed simply by inspection, but if automatic criteria are required (for example if optimising the force–displacement profile for a given application) it is sufficient to ensure that:

- $\mathrm{d}^3\hat{P}/\mathrm{d}\hat{z}^3\big|_{\hat{z}_{k_{\min}}} > 0$ to ensure that Eq. (11) gives a minimum not a maximum and that
- the region of expected operation is free from any regions of negative stiffness, to prevent bistable responses that are not modelled and would be unwelcome in a practical mount.

2.4. Translation of the system due to constant acceleration

The effect of a constant acceleration of the base, altering the static equilibrium position of the mass relative to the base, is now considered. To simplify dynamic calculations, the equation of motion (Eq. (5)) is translated for motions about the new static equilibrium position.

The constant acceleration is expressed in terms of the gravitational acceleration g as Δg where Δ is a real constant. Considering just this constant acceleration, $\ddot{r} = \Delta g$ is substituted into Eq. (1). It is assumed that the static force is due to the weight of the mass, i.e. $F_s = mg$, and the system is in static equilibrium so that $\hat{z}'' = \hat{z}' = 0$. Substitution of these assumptions into Eqs. (2)–(5) allows the constant displacement from the original equilibrium position $\hat{Z}_c$ to be calculated by solving

$$\hat{P}(\hat{Z}_c) = -\Delta \tag{14}$$

To facilitate the dynamic analysis, Eq. (5) is changed to use the translated variable $\tilde{z} = \hat{z} - \hat{Z}_c$, giving

$$\tilde{z}'' + 2\lambda\tilde{z}' + N_z(\tilde{z}) = -\tilde{r}'' \tag{15}$$

where $\tilde{r}'' = \hat{r}'' - \Delta$ and

$$\tilde{P}(\tilde{z}) = \hat{P}(\tilde{z} + \hat{Z}_c) = \tilde{k}_1\tilde{z} + \tilde{k}_2\tilde{z}^2 + \tilde{k}_3\tilde{z}^3 + \tilde{k}_4\tilde{z}^4 + \tilde{k}_5\tilde{z}^5 \tag{16}$$

The constants $\tilde{k}_n$ may be found from the Taylor expansion of $\hat{P}(\tilde{z})$ about zero, evaluated at $\hat{Z}_c$.

2.5. Excitation

The oscillatory part of the base motion is assumed to be a harmonic signal with amplitude $\tilde{R}$ and phase difference ϕ, hence

$$\tilde{r}'' = -\hat{\Omega}^2\tilde{R}\cos(\hat{\Omega}\tau + \phi) \tag{17}$$

where $\hat{\Omega} = \Omega/\omega_s$. This is representative of a typical situation, where there is a source of vibration that is dominated by a single frequency, such as in the vicinity of a motor. Note that the phase difference ϕ has been applied to the excitation instead of the response to simplify calculations, and will be determined later. Substituting Eq. (17) into Eq. (15) gives

$$\tilde{z}'' + 2\lambda\tilde{z}' + \tilde{P}(\tilde{z}) = \Omega^2\tilde{R}\cos(\hat{\Omega}\tau + \phi) \tag{18}$$

2.6. Normal forms analysis

The steady-state solutions to Eq. (18) are found using the method of normal forms [21]. The full details are given in Appendix A, however a brief outline of the method is given here.

The method transforms Eq. (18) to the form

$$u'' + 2\lambda u' + \omega_n^2 u + N_u(u) = \Omega^2\tilde{R}\cos(\hat{\Omega}\tau + \phi) \tag{19}$$

where $\tilde{z} = u + h(u)$, and $h(u) \ll u$ so that u is an approximation to $\tilde{z}$. In this work, U represents the amplitude of the component of $\tilde{z}$ that is at the forcing frequency whereas $h(u)$ represents the response at harmonics of the forcing frequency. The natural frequency ω_n used in Eq. (19) is an estimate that may be found in various ways. Unlike Eq. (18), Eq. (19) may be solved exactly on substitution of a trial solution of form $u = U\cos(\hat{\Omega}\tau)$. The determination of $N_u(u)$ and $h(u)$ occurs alongside the substitution of this trial solution, and results in $N_u(u)$ having the form

$$N_u(u) = \sum C_s U^s \cos(\hat{\Omega}\tau) \tag{20}$$

This is substituted into Eq. (19), and the result split into real and imaginary components of $\cos(\omega t)$:

$$-\hat{\Omega}^2 U + \omega_n^2 U + \mathrm{Re}\left(\sum C_s U^s\right) = -\tilde{R}\hat{\Omega}^2\cos\phi \tag{21}$$

$$-2\lambda\hat{\Omega}U + \mathrm{Im}\left(\sum C_s U^s\right) = -\tilde{R}\hat{\Omega}^2\sin\phi \tag{22}$$

To eliminate ϕ, both equations are squared and summed, resulting in a polynomial in U for a given $\hat{\Omega}$, which can be solved to give U. ϕ can then be resolved from either equation.

When U has been determined, the transformation $h(u)$ can be evaluated, and this is used to determine harmonic responses of the form $H_q\cos(q\hat{\Omega})$. In this work, H_2 and H_0 (time-constant response) are seen to be potentially significant.

Finally, the amplitude of absolute displacement $\hat{X}_1$ may be determined from phasor addition of u and the forcing signal.

3. Results and discussion

3.1. Symmetric HSLDS mounts subject to constant acceleration term

Results are presented for two symmetric stiffness mounts, with force displacement curves shown in Fig. 3. The first of these has a very low equilibrium stiffness of $\hat{k}_e = 0.01$, and shall be referred to as a Quasi-Zero Stiffness (QZS) mount, a term suggested by Carrella in [9]. The other has a more moderately reduced equilibrium stiffness of $\hat{k}_e = 0.25$, and shall be referred to as simply a Reduced Stiffness (RS) mount.

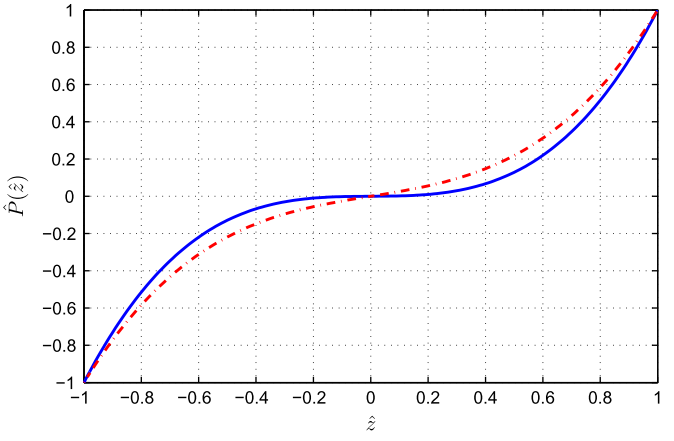

Fig. 3. Force displacement curves of two symmetric stiffness mounts; a mount with $\hat{k}_e = 0.01$ (solid line) referred to as the Quasi-Zero Stiffness (QZS) mount, and a mount with $\hat{k}_e = 0.25$ (dot-dash line) known as the Reduced Stiffness (RS) mount. For both mounts, $\hat{z}_r = \sqrt{1/3}$, $\hat{z}_{k_{\min}} = 0$ and $\hat{F}_{z_s+} = 1$.

Figs. 4 and 5 show the effect of the constant acceleration term Δ on the steady-state dynamic response of these mounts. Firstly, consider Fig. 4 which shows the response of the QZS mount, as shown by the solid line in Fig. 3. It can be seen that when $\Delta = 0$, this is an excellent isolator, with a low natural frequency and peak amplitude (compared to the equivalent linear system which has a peak response at $\Omega = 1$), and consequently a low isolation frequency. However as Δ increases, the peak amplitude and frequency increase dramatically; they remain below that of the equivalent linear system, but are far greater than the designed performance. Note also that the response peaks now soften with amplitude rather than stiffen. This softening effect is beneficial when in resonance, because increases in peak amplitude are mitigated by reductions in peak frequency; however note from the low amplitude response that it confers no advantage to the isolation frequency. From the lower subplot it may be seen that a significant H_0 term (see Eq. (A.23), denoting a constant offset in addition to that caused by the static effect of Δ alone, develops. This shows that the centre of oscillation tends to head towards the point of minimum stiffness at higher amplitudes. The magnitude of H_2 shows that second-order harmonics are now significant in relation to the fundamental response; contrast this with symmetric mounts under design conditions where only third- and fifth-order harmonics exist, and these are seldom of significant magnitude as shown in [20]. The magnitudes of the terms H_0 and H_2 mean that these cases approach the limits of our assumption that these terms remain small (see (A.6)), and indeed at higher levels of forcing errors are seen to occur.

Compare this to the performance of the RS isolator of Fig. 3. Fig. 5 shows that both the peak frequency and amplitude are reduced by around 40 percent under designed conditions, so the RS mount gives substantially less isolation than the QZS mount when under design conditions. This system is still adversely affected by the constant acceleration, but by a relatively smaller amount, with the response hardly changing at all for $\Delta \leq 0.025$. Comparing Fig. 5 to Fig. 4, it can be seen that the

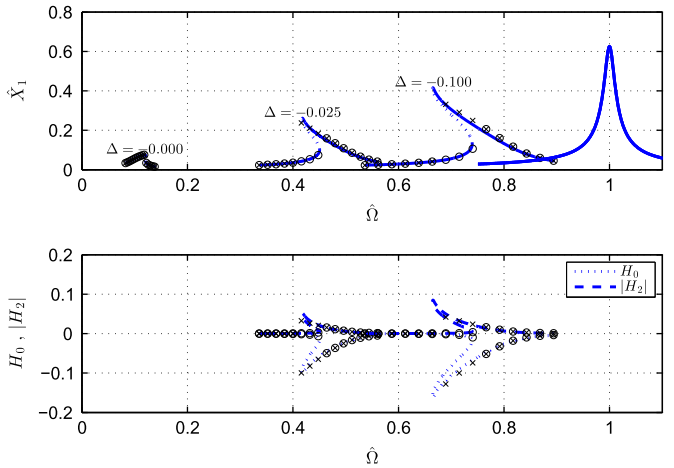

Fig. 4. Steady-state responses of the QZS mount, subjected to harmonic base excitation and with constant acceleration term Δ. Line shows analytical solution, with a dotted line on the upper graph indicating unstable regions of response. Markers show results from numerical simulation of a stepped sine frequency sweep; ○ indicates a sweep in the positive frequency direction, × indicates the negative frequency direction. Peak at right of upper graph shows the equivalent linear system response for comparison. $\hat{k}_e = 0.01$, $\hat{z}_r = \sqrt{1/3}$, $\hat{z}_{k_{\min}} = 0$, $\hat{F}_{z_s+} = 1$, $\lambda = 0.01$, $\hat{R} = 0.0125$.

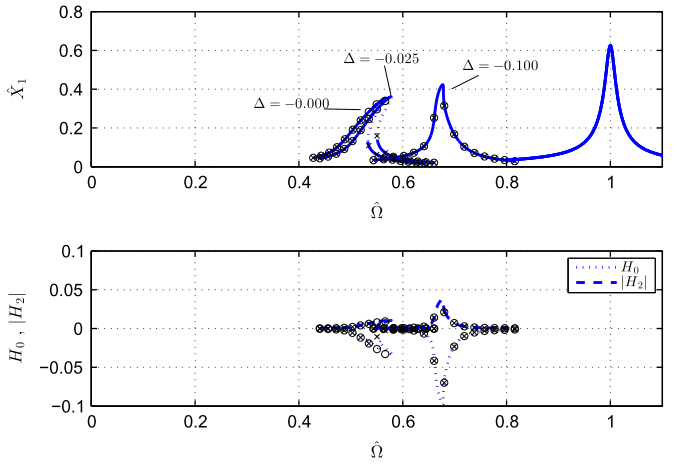

Fig. 5. Steady-state responses of the RS mount, subjected to harmonic base excitation and with constant acceleration term Δ. Lines and markers have the same meaning as Fig. 4. $\hat{k}_e = 0.25$, $\hat{z}_r = \sqrt{1/3}$, $\hat{z}_{k_{\min}} = 0$, $\hat{F}_{z_s+} = 1$, $\lambda = 0.01$, $\hat{R} = 0.0125$.

QZS mount will often provide diminished isolation when even a small constant acceleration term is present. At $\Delta \leq 0.025$, the peak amplitude and frequency are similar between the RS and QZS mounts, but the RS mount's response has a significantly smaller 2nd harmonic. It may also be noted that the RS mount has slightly smaller constant displacement term $\hat{Z}_0$ than the QZS mount. In summary, Figs. 4 and 5 show that when static loading errors are present, the QZS mount has little or no advantage over the RS mount and may even perform worse.

3.2. Designed performance of asymmetric HSLDS mounts

In this section, the performance of mounts with stiffness asymmetries, whilst operating about their designed equilibrium (i.e. with $\Delta = 0$) is considered. The force displacement curves of four such mounts are shown in Fig. 6, where the asymmetric shape parameters $\hat{z}_{k_{\min}}$ and $\hat{F}_{z_s+}$ have been varied.

The steady-state frequency responses of the mounts shown in Fig. 6 are shown in Fig. 7. This shows that for each of these mounts, a small reduction in peak frequency is observed compared to the symmetric stiffness mount ($\hat{z}_{k_{\min}} = 0$, $\hat{F}_{z_s+} = 1$), when no static loading error exists. This is because, by reducing the amount of stiffening in the positive $\hat{z}$ region, the mount experiences less hardening with increasing amplitude. These responses are accompanied by small positive H_0 terms as seen in the lower part of Fig. 7, showing that the mounts have a slight tendency to move towards their points of minimum stiffness when the amplitude of oscillation is large. Despite the presence of the second polynomial terms in the force displacement curves of these mounts, second-order harmonic responses remain small. Due to the slightly lower peak frequency and amplitude of the asymmetric mounts, it may be said that they are an improvement on the symmetric mount. There is little apparent difference between the form of asymmetry ($\hat{z}_{k_{\min}}$ or $\hat{F}_{z_s+}$) that is altered in this case.

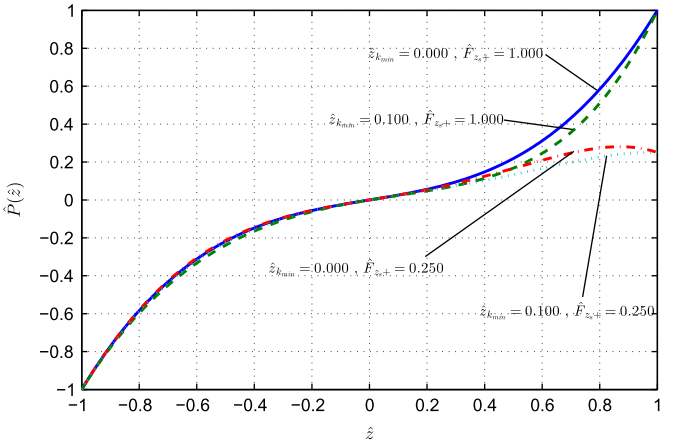

Fig. 6. Force displacement curves for asymmetric mounts. $\hat{k}_e = 0.25$, $\hat{z}_r = \sqrt{1/3}$.

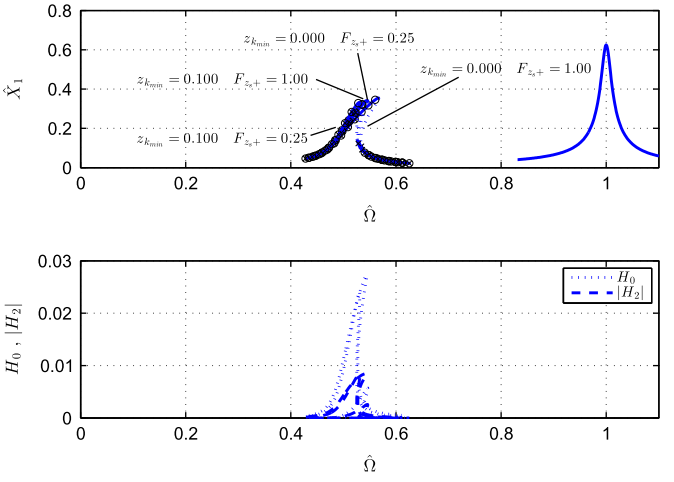

Fig. 7. Steady-state responses of an HSLDS mount with asymmetrical stiffness, subjected to harmonic base excitation. Lines and markers have the same meaning as Fig. 4. $\Delta = 0.0$, $\hat{k}_e = 0.25$, $\hat{z}_r = \sqrt{1/3}$, $\lambda = 0.01$, $\hat{R} = 0.0125$.

3.3. Asymmetric HSLDS mounts with constant acceleration

This section considers the effect of the constant acceleration term Δ on the same mounts as described in the previous section, with force displacement curves shown in Fig. 6. Fig. 8 shows the steady-state response of the asymmetric stiffness mounts subject to harmonic base excitation and a constant acceleration.

In this case, setting $\hat{z}_{k_{\min}} = 0.1$ and $F_{z_s+} = 0.25$ both have the effect of reducing both peak frequency and amplitude, and making both of these change together has an even greater benefit. The case with both $\hat{z}_{k_{\min}} = 0.1$ and $F_{z_s+} = 0.25$ ameliorates much of the loss in performance due to the constant acceleration Δ.

Another point of interest is shown by the backbone curves in Fig. 8. These are given by the solutions of Eq. (A.27) with no forcing or damping present. At the amplitude shown, the asymmetric mounts have a gently softening trend, whereas the symmetric mounts have a significantly hardening trend. For the asymmetric mounts, small increases in the peak amplitude are slightly compensated for by a reduction in peak frequency; whereas for the symmetric mounts they incur an increase in peak frequency. This means that the asymmetric mounts' resonant behaviour is less sensitive to changes in damping or excitation, which in practice are both susceptible to errors in prediction and measurement. This would be a significant aid to the design of a mount where resonant behaviour is a constraint.

It may also be noted that the second harmonic amplitudes are much smaller in the asymmetric cases than in the symmetric cases. Therefore, despite the symmetric stiffness mount having no even harmonics under ideal conditions, in realistic operating conditions when loading error is present they will frequently exhibit significantly greater 2nd harmonics than the asymmetric mounts.

Finally, Fig. 9 shows the influence of the different choices of shape parameters on the isolation region. It is clear that all mounts give much better isolation for frequencies up to 100 times the natural frequency of the equivalent linear system. However the best of the mounts discussed, that with $F_{z_s+} = 0.25$ and $\hat{z}_{k_{\min}} = 0.1$, maintains a noticeable advantage over the others until approximately 20 times the equivalent linear frequency. Therefore the changes described in the resonant region lead to benefits in the isolation region as well.

Clearly the advantages described above are only realised when Δ has a negative sign, corresponding to an overload of the mount; if this cannot be anticipated the asymmetric stiffness will be of little benefit. However there are many situations where this assumption may be made; for example in transport aircraft it may be anticipated that apparent g will often be raised for significant periods due to manoeuvres such as banked turns; however periods of reduced g are generally only transitory. Alternatively, the intended equilibrium point may be chosen differently, so that it lies at the midpoint of the region of acceptable performance created by asymmetry, thereby allowing negative or positive errors.

3.4. Comparing a symmetric and asymmetric mount over a range of operating conditions

Using the resonance conditions described in Appendix A.6, it is possible to create a surface plot of the peak frequency for a given mount at a wide range of operating conditions. The peak frequency $\hat{\omega}_0$, nondimensionalised by the natural frequency of the equivalent linear system, is an important characteristic of a mount, and Eq. (A.26) shows that it is directly related to peak amplitude.

The result of this is shown in Fig. 10 for two mounts, one symmetric and the other asymmetric, over a range of base excitation amplitudes and levels of constant acceleration Δ. The base amplitude is presented in terms of the ratio $\tilde{R}/\lambda$, which due to Eq. (A.26) gives equivalent responses over a range of systems in resonance; further details on this relationship may be

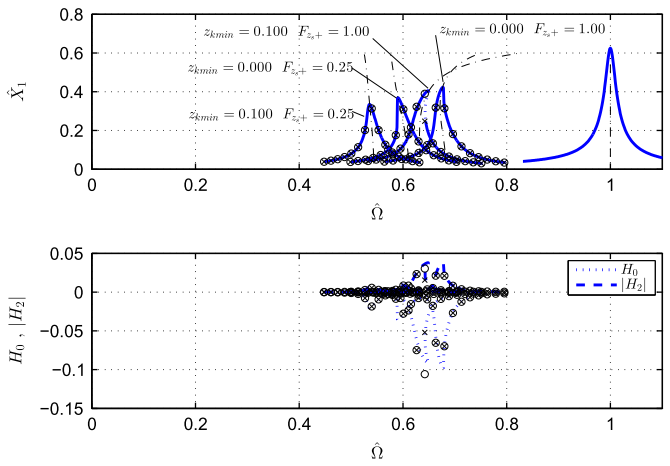

Fig. 8. Steady-state responses of RA mount with symmetrical stiffness compared to asymmetric stiffness mounts, subjected to harmonic base excitation and with constant acceleration term $\Delta = 0.1$, $\hat{k}_e = 0.25$, $\lambda = 0.01$, $\hat{R} = 0.015$. Lines and markers have the same meaning as Fig. 4, with the addition that the dot-dash line represents the backbone curve of the response.

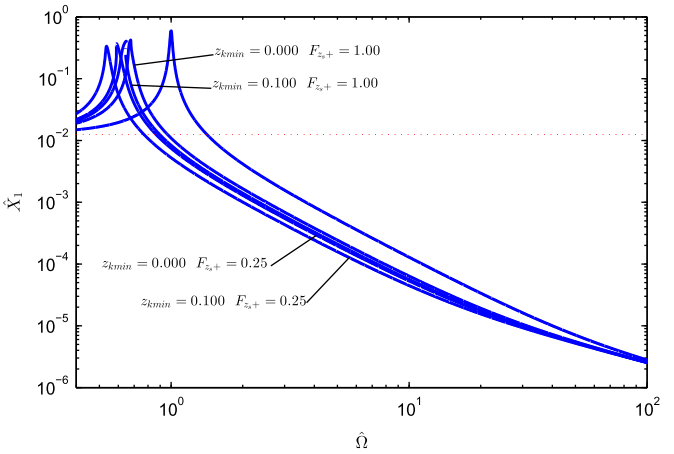

Fig. 9. Log plot of steady state responses (solid lines) of HSLDS mounts with symmetrical and asymmetric stiffness, subjected to harmonic base excitation and with constant acceleration term $\Delta = 0.1$, $\hat{k}_e = 0.25$, $\lambda = 0.01$, $\hat{R} = 0.015$. Right hand peak shows the equivalent linear system response, red dotted line shows base amplitude. (For interpretation of the references to colour in this figure caption, the reader is referred to the web version of this paper.)

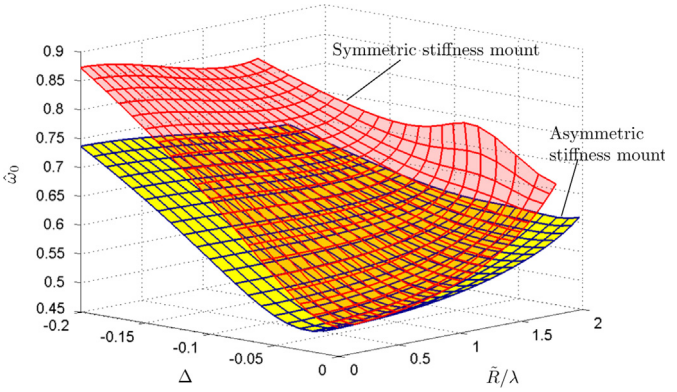

Fig. 10. Surface plots of peak frequency for two different HSLDS systems, with nondimensional peak response frequency $\hat{\omega}_0$ plotted against the constant acceleration term Δ and the ratio of nondimensional base amplitude to the damping ratio of the equivalent linear system $\tilde{R}/\lambda$. The upper plot is a symmetric system: $\hat{k}_e = 0.25$, $\hat{z}_r = \sqrt{1/3}$, $\hat{F}_{z_s+} = 1$, $\hat{z}_{k_{\min}} = 0$. The lower plot is asymmetric with $\hat{k}_e = 0.25$, $\hat{z}_r = 0.577$, $\hat{F}_{z_s+} = 0.5$, $\hat{z}_{k_{\min}} = 0.1$.

found in [20]. The range of $\tilde{R}/\lambda$ shown encompasses most of the range over which the symmetric stiffness mount gives useful frequency reduction.

As can clearly be seen, whilst both systems have identical performance at $\Delta = \tilde{R}/\lambda = 0$, the symmetric mount experiences greater peak frequency (and therefore also greater peak amplitude) far more rapidly as constant acceleration and excitation increase. This demonstrates that an asymmetric stiffness mount can perform with a lower peak frequency (and therefore peak amplitude) than a symmetric mount over a wide range of operating conditions. However, this advantage is clearly dependent on being able to anticipate that Δ is negative; if Δ were to be positive, the two mounts would have similar performance as both would oscillate in negative $\hat{z}$ region of Fig. 6 where their force–displacement curves are similar.

4. Conclusions

This work has shown that loading errors in the form of a constant acceleration of the base, expressed as a factor of gravitational acceleration, can be a major impairment to the performance of HSLDS isolators with symmetric stiffness. The reduction in performance is relatively more acute for Quasi-Zero Stiffness isolators, suggesting that in many cases such mounts will perform little, if at all, better than more moderately nonlinear mounts if static loading cannot be accurately controlled.

Asymmetric stiffness can improve the performance of an HSLDS mount when operating about its designed static equilibrium position. In addition, asymmetric stiffness can be particularly advantageous if designed to anticipate the likely sign of the loading error, and reduce the rate of stiffening experienced in that direction. In these cases, they can ameliorate much of the reduction in isolation performance caused by the loading error. Furthermore the resulting resonant responses are less sensitive to changes in excitation or damping, reducing the effect of errors in these properties.

When loading errors are present, HSLDS mounts produce second harmonic components in the resonant region, adding to the large vibrations at the fundamental frequency. It was found that mounts with appropriately designed asymmetry can significantly reduce this problem as well.

The results of this study can be used to compare the dynamic performances of HSLDS isolators with different nonlinear mechanisms and force–displacement curves, using the idealisations given above. The results may also be used to optimise designs of vibration isolators for particular applications, wherever the nonlinearity may be controlled to tailor an optimal force–displacement curve.

Acknowledgements

The research leading to these results has received funding from the European Research Council under the European Union's Seventh Framework Programme (FP/2007-2013)/ERC Grant Agreement no. [247045], and also from EPSRC Grant no. EP/G036772/1. In addition, Simon Neild is supported by an EPSRC Fellowship (EP/K005375/1).

Appendix A. Solution of steady state response to harmonic base excitation

A.1. Overview of method

Time simulation of Eq. (18) shows that the systems of concern in this work frequently encounter steady-state responses with significant components that are time-constant (in addition to the term $\hat{Z}_c$ calculated already), and also at double the excitation frequency. These steady-state solutions are found analytically with a Normal Forms (NF) method for second-order differential Eqs. [22–25]. This method transforms Eq. (18) to a nearly identical form that may be exactly solved as a polynomial equation of the fundamental amplitude. The transformation itself then yields information on the time constant and harmonic terms unlike the Harmonic Balance (HB) method [21,26] which discards any terms that are not matched.

The method proceeds in the following way. Firstly, Appendix A.2 defines the form of the transformation, and how accuracy of the transformed system can be established. Then, in Appendix A.3, a solution form is assumed, resulting in an expansion of terms which is given in matrix form for convenience. The transformation is defined in the form of rules for how each term should be handled. Once the transformation is performed, Appendix A.4 shows how the resulting frequency response equation may be solved exactly, and how the harmonics may be estimated. Finally, since Eq. (18) defines displacement in relative terms, the means of obtaining the absolute displacements is described in Appendix A.5.

A.2. Normal form solution approximation for second-order differential equations

Firstly, Eq. (18) is recast as

$$\tilde{z}'' + 2\lambda\tilde{z}' + \omega_n^2\tilde{z} + N_z(\tilde{z}) = \Omega^2\tilde{R}\cos(\hat{\Omega}\tau + \phi) \tag{A.1}$$

where $N_z(\tilde{z}) = \tilde{P}(z) - \omega_n^2\tilde{z}$ and ω_n is the natural frequency of the nonlinear system. Estimating ω_n as the linearised natural frequency, given by $\omega_n^2 = \tilde{k}_1$, will give reasonable accuracy for weak nonlinearity, but a refined estimate that reflects the softening or stiffening of the response can improve the prediction accuracy of harmonic responses as shown in [24]. A means of obtaining a refined estimate is obtained in Appendix A.6, and used in the results in this work.

The Normal Form method determines a transformed variable u given by

$$\tilde{z} = u + h(u) \tag{A.2}$$

where $h(u) \ll u$ so that u is a reasonable approximation to $\tilde{z}$, and hence the transformation may be described as a near-identity transformation. The transformation, which removes non-resonant terms, is such that the transformed equation of motion has the form

$$u'' + 2\lambda u' + \omega_n^2 u + N_u(u) = \hat{\Omega}^2\tilde{R}\cos(\hat{\Omega}\tau + \phi) \tag{A.3}$$

and can be solved exactly, whereupon harmonics can be found from the transformation function $h(u)$.

Firstly, Eq. (A.3) is subtracted from Eq. (A.1), and Eq. (A.2) is substituted to obtain the relationship between the original equation, the transformed equation and the transformation itself:

$$h(u)'' + 2\lambda h(u)' + \omega_n^2 h(u) + N_z(\tilde{z}) - N_u(u) = 0 \tag{A.4}$$

This equation is important because it represents the physical accuracy of the method in terms of force; if it is solved exactly our transformed solution exactly meets the balance of forces in Eq. (18).

However, the term $N_z(z)$ must be approximated in terms of u and $h(u)$. To do this, $h(u)$ is broken down into

$$h(u) = h_1(u) + h_2(u) \tag{A.5}$$

where $h_2(u) \ll h_1(u)$. $N_z(\tilde{z})$ is then approximated using a Taylor series:

$$N_z(\tilde{z}) \approx N_z(u) + h_1(u)\left.\frac{\mathrm{d}N_z}{\mathrm{d}\tilde{z}}\right|_u \tag{A.6}$$

where the truncation error is of order $\mathcal{O}\left(h_1(u)^2, h_2(u)\right)$. Hence $h_2(u)$ represents very small terms that are crudely approximated, while $h_1(u)$ represents terms that are larger but approximated more accurately.

A.3. Normal Form transformation

The Normal Form transformation is the process of determining $N_u(u)$, $h_1(u)$ and $h_2(u)$ and is done simultaneously with the substitution of a trial solution. The trial solution for u is given in the form

$$u = U\cos(\hat{\Omega}\tau) = u_p + u_m \tag{A.7}$$

where the notation $u_p = (U/2)\mathrm{e}^{\mathbf{i}\Omega\tau}$ and $u_m = (U/2)\mathrm{e}^{-\mathbf{i}\Omega\tau}$ is used to facilitate the forthcoming computations. Note that the trial solution assumes that response is predominately at the forcing frequency $\hat{\Omega}$, an assumption that is confirmed in all the cases studied here. Furthermore, recall that phase difference has already been handled in the forcing function equation (17), hence its absence from the assumed solution.

Now consider the trial solution substituted into an example expression αu^2:

$$\alpha u^2 = \alpha\left(u_p^2 + 2u_p u_m + u_m^2\right) = [\alpha \;\; 2\alpha \;\; \alpha]\begin{bmatrix} u_p^2 \\ u_p u_m \\ u_m^2 \end{bmatrix} \tag{A.8}$$

From this example it may be seen that any polynomial term of the trial solution can be expressed as the product of a row vector of constants and a column vector which consists of functions of U, $\hat{\Omega}$ and time of form $u_p^i u_m^j$.

Time derivatives of polynomial terms can be shown in a similar format, by multiplying a diagonal matrix of $n\mathbf{i}\hat{\Omega}$ terms. For example:

$$\frac{\mathrm{d}}{\mathrm{d}\tau}\alpha u^2 = [\alpha \;\; 2\alpha \;\; \alpha]\begin{bmatrix} 2\mathbf{i}\hat{\Omega} & 0 & 0 \\ 0 & 0 & 0 \\ 0 & 0 & -2\mathbf{i}\hat{\Omega} \end{bmatrix}\begin{bmatrix} u_p^2 \\ u_p u_m \\ u_m^2 \end{bmatrix} \tag{A.9}$$

The term in the diagonal matrix associated with a term $u_p^i u_m^j$ in the column vector is given by

$$\hat{\omega}_{(i,j)} = \mathbf{i}\hat{\Omega}(i-j) \tag{A.10}$$

Higher time derivatives are simply found by repeatedly applying the square matrix.

The above examples motivate the definition of a vector $\mathbf{u}^*$ defined as

$$\mathbf{u}^* = \left[u_p^1 u_m^0 \;\; u_p^0 u_m^1 \;\; u_p^2 u_m^0 \;\; u_p^1 u_m^1 \;\; u_p^0 u_m^2 \;\; u_p^3 u_m^0 \;\; \ldots \;\; u_p^0 u_m^P\right]^T \tag{A.11}$$

which consists of all combinations of i and j that will appear in the solution. The highest exponent P is determined by the term $h_1 \mathrm{d}N_z/\mathrm{d}z|_u$ in Eq. (A.6) by assuming that $h_1(u)$ has the same polynomial order N as $N_z(u)$. The derivative will have order $N-1$, hence the product of these terms will be a polynomial of order

$$P = 2N - 1 \tag{A.12}$$

The following terms from Eqs. (A.6) and (A.4) may now be represented with a matrix product notation:

$$\begin{gathered} h_1(u) = \mathbf{h_1}\mathbf{u}^*, \quad h_2(u) = \mathbf{h_2}\mathbf{u}^*, \quad N_u(u) = \mathbf{N_u}\mathbf{u}^* \\ h(u) = \mathbf{h}\mathbf{u}^*, \quad h(u)' = \mathbf{h}\hat{\boldsymbol{\omega}}\mathbf{u}^*, \quad h(u)'' = \mathbf{h}\hat{\boldsymbol{\omega}}^{\mathbf{2}}\mathbf{u}^* \\ N_z(u) = \mathbf{N_z}\mathbf{u}^*, \quad \left.\frac{\mathrm{d}N_z}{\mathrm{d}\tilde{z}}\right|_u = \mathbf{dN_z}\mathbf{u}^* \end{gathered} \tag{A.13}$$

where $\mathbf{h_1}$, $\mathbf{h_2}$ and $\mathbf{N_u}$ are $1 \times P$ horizontal matrices to be determined, $\mathbf{h} = \mathbf{h_1} + \mathbf{h_2}$, $\hat{\boldsymbol{\omega}}$ is a $P \times P$ diagonal matrix in the manner of that in Eq. (A.9), $\hat{\boldsymbol{\omega}}^{\mathbf{2}} = \hat{\boldsymbol{\omega}}\hat{\boldsymbol{\omega}}$, $\mathbf{N_z}$ is $1 \times P$ horizontal matrix determined by expanding $N_z(u)$ in the manner of Eq. (A.8), and $\mathbf{dN_z}$ is a similar matrix obtained from an expansion of $\mathrm{d}N_z/\mathrm{d}\tilde{z}|_u$. One final term is required that needs special treatment because it involves products of $\mathbf{u}^*$ terms

$$h_1(u)\left.\frac{\mathrm{d}N_z}{\mathrm{d}\tilde{z}}\right|_u = (\mathbf{h_1}\mathbf{u}^*)\cdot(\mathbf{dN_z}\mathbf{u}^*) = \mathbf{M}\mathbf{u}^* \tag{A.14}$$

A term of $\mathbf{M}$ is given by

$$M_{(i,j)} = \sum_{\substack{a+c=i \\ b+d=j}} h_{1(a,b)}\mathrm{d}N_{(c,d)} \tag{A.15}$$

where $h_{1(a,b)}$ and $dN_{(c,d)}$ are terms from $\mathbf{h_1}$, $\mathbf{dN_z}$ respectively and the bracketed subscripts (i,j) indicate that a term corresponds to an element of $\mathbf{u}^*$ with $u_p^i u_m^j$, and subscripts (a,b) and (c,d) have a similar meaning to subscripts (i,j).

Substitution of Eqs. (A.5), (A.6), (A.11), (A.13) and (A.14) into Eq. (A.4) gives

$$\begin{aligned}&\mathbf{h_1}\hat{\omega}^2\mathbf{u}^*+2\lambda\mathbf{h_1}\hat{\omega}\mathbf{u}^*+\omega_n^2\mathbf{h_1}\mathbf{u}^*\\&+\mathbf{h_2}\hat{\omega}^2\mathbf{u}^*+2\lambda\mathbf{h_2}\hat{\omega}\mathbf{u}^*+\omega_n^2\mathbf{h_2}\mathbf{u}^*\\&+\mathbf{N_z}\mathbf{u}^*+\mathbf{M}\mathbf{u}^*-\mathbf{N_u}\mathbf{u}^*=0\end{aligned}\tag{A.16}$$

This can be solved term-by-term as P equations in the form

$$\begin{aligned}&h_{1(i,j)}\hat{\omega}^2+2\lambda h_{1(i,j)}\hat{\omega}_{(i,j)}+\omega_n^2 h_{1(i,j)}\\&+h_{2(i,j)}\hat{\omega}_{(i,j)}^2+2\lambda h_{2(i,j)}\hat{\omega}_{(i,j)}+\omega_n^2 h_{2(i,j)}\\&+N_{z(i,j)}+M_{(i,j)}-N_{u(i,j)}=0\end{aligned}\tag{A.17}$$

where a similar convention to Eq. (A.15) is used. Note that it is necessary to proceed in ascending order of the overall power given by $i+j$, as this ensures that the relevant terms to compute Eq. (A.15) will have been evaluated. There are infinitely many solutions of Eq. (A.17), by varying $h_{1(i,j)}$, $h_{2(i,j)}$ or $N_{u(i,j)}$. However the following rules are used to restrict this choice:

1. If $i+j$ is greater than N, h_1 is zero, otherwise h_2 is zero. This has the effect that h_1 contains terms up to the Nth power of U, and h_2 has higher powers up to the Pth power.
2. It is preferable to have $N_u(u)$ as small as possible to keep Eq. (A.3) simple. Therefore, the default action is to set $N_{u(i,j)}=0$ and have

$$h_{n(i,j)}=\frac{-N_{z(i,j)}-M_{(i,j)}}{\hat{\omega}_{(i,j)}^2+2\lambda\hat{\omega}_{(i,j)}+\omega_n^2}\tag{A.18}$$

   where n is 1 or 2 according to rule 1. Note that this term is small whenever $|\hat{\omega}_{(i,j)}|$ differs significantly from ω_n, satisfying the assumption of a near identity transformation.
3. However if $|i-j|=1$, Eq. (A.10) leads to $\hat{\omega}_{(i,j)}^2+\omega_n^2\approx 0$, so that the denominator in Eq. (A.18) is small when forcing is near resonance. Therefore $h_{n(i,j)}$ is large and violates the assumption of a near identity transformation. In these cases the term must be included in Eq. (A.3), so Eq. (A.17) is solved by $h_{n(i,j)}=0$ and $N_{u(i,j)}=N_{z(i,j)}+M_{(i,j)}$.

A.4. Definition and solution of the frequency response equation

Once the above rules have been applied for all terms in $\mathbf{u}^*$, in ascending order of the overall power, and with a given forcing frequency, all matrices will be populated. It is now possible to solve the resonant equation, Eq. (A.3). $N_u(u)$ can be rearranged into the following form:

$$N_u(u)=\mathbf{N_u}\mathbf{u}^*=\sum C_s U^s\cos(\hat{\Omega}\tau)\tag{A.19}$$

where C_s is a complex coefficient given by

$$C_s=\sum_{i+j=s}\frac{N_{u(i,j)}}{2^s}\tag{A.20}$$

This can now be substituted into Eq. (A.3), and the result split into real and imaginary components of $\cos(\hat{\Omega}t)$:

$$-\hat{\Omega}^2U+\omega_n^2U+\mathrm{Re}\left(\sum C_sU^s\right)=-\tilde{R}\hat{\Omega}^2\cos\phi\tag{A.21}$$

$$-2\lambda\hat{\Omega}U+\mathrm{Im}\left(\sum C_sU^s\right)=-\tilde{R}\hat{\Omega}^2\sin\phi\tag{A.22}$$

To eliminate ϕ, both equations are squared and summed, resulting in a polynomial in U for a given $\hat{\Omega}$, which can be solved to give U. ϕ can then be resolved from either equation.

Eq. (A.18) can now be evaluated to get the transformation functions, but more usefully it can derive the qth harmonic given by $H_q\cos(q\hat{\Omega})$ where

$$H_q=\sum_{|i-j|=q}h_{(i,j)}\tag{A.23}$$

The amplitude is the modulus of H_q and the phase relative to the fundamental response is given by $\angle H_q$.

A.5. Absolute motion of mass

The transformed variable U represents the component of the relative displacement of the mass at the fundamental frequency. It is often desirable to obtain the fundamental component amplitude of the absolute displacement, which is

obtained by phasor addition of U and the base motion:

$$\hat{X}_1 = \sqrt{\left(U+\tilde{R}\cos\phi\right)^2 + \left(\tilde{R}\sin\phi\right)^2} \tag{A.24}$$

The overall constant displacement due to the vibration and to the acceleration term is given by

$$\hat{X}_0 = \hat{Z}_c + H_0 \tag{A.25}$$

All other harmonic components of the absolute response are identical to their counterparts in the relative response, as estimated by Eq. (A.23).

A.6. Resonance conditions and improved values for ω_n^2

In many cases it is unnecessary to obtain a full frequency response for a system, and it is more useful to gain general insight into the relationship between peak frequency, peak amplitude and other system parameters. To obtain these relationships, it is assumed that the system is in resonance and that therefore the phase angle $\phi = \pi/2$. This condition is substituted into Eq. (A.22) leading to

$$-2\lambda U\hat{\Omega} + \Im\mathrm{m}\left(\sum C_s U^s\right) = -\tilde{R}\hat{\Omega}^2$$

where it emerges that the summation term is zero when only stiffness nonlinearities are present, giving the simple relation

$$U = \frac{\tilde{R}}{2\lambda}\hat{\Omega} \tag{A.26}$$

when at resonance. Similar assumptions in Eq. (A.21) lead to

$$-\hat{\Omega}^2 U + \omega_n^2 U + \Re\mathrm{e}\left(\sum C_s U^s\right) = 0 \tag{A.27}$$

Therefore $\hat{\Omega}$ when in resonance can be determined for any given U by solving Eq. (A.27) with a nonlinear solver (recalling that C_s terms will alter with different trial values for $\hat{\Omega}$). This can be related back to the excitation and damping by the use of Eq. (A.26). The unforced and undamped solutions of Eq. (A.27) give the so-called backbone curve [21].

Therefore the true nonlinear resonant frequency can be obtained, and this value may be used for ω_n in all other calculations if $N_z(z)$ is updated as per Eq. (A.1). This leads to improvements in accuracy as demonstrated in [24]. Further detail on this topic may also be found in [27].

References

[1] D.J. Mead, *Passive Vibration Control*, John Wiley and Sons, Chichester, United Kingdom, 1999.
[2] A. Carrella, *Passive Vibration Isolators with High-Static-Low-Dynamic-Stiffness*, VDM Verlag Dr. Muller, Saarbrücken, Germany, 2010.
[3] J. Winterflood, D.G. Blair, B. Slagmolen, High performance vibration isolation using springs in euler column buckling mode, *Physics Letters A* 300 (2–3) (2002) 122–130.
[4] L.N. Virgin, R.B. Davis, Vibration isolation using buckled struts, *Journal of Sound and Vibration* 260 (5) (2003) 965–973.
[5] R.H. Plaut, J.E. Sidbury, L.N. Virgin, Analysis of buckled and pre-bent fixed-end columns used as vibration isolators, *Journal of Sound and Vibration* 283 (3–5) (2005) 1216–1228.
[6] L.N. Virgin, S.T. Santillan, R.H. Plaut, Vibration isolation using extreme geometric nonlinearity, *Journal of Sound and Vibration* 315 (3) (2008) 721–731.
[7] S.T. Santillan, Analysis of the elastica with applications to vibration isolation, PhD Thesis, Department of Mechanical Engineering and Materials Science, Duke University, 2007.
[8] R. DeSalvo, Passive, nonlinear, mechanical structures for seismic attenuation, *Journal of Computational and Nonlinear Dynamics* 2 (4) (2007) 290–298.
[9] A. Carrella, M.J. Brennan, T.P. Waters, Static analysis of a passive vibration isolator with quasi-zero-stiffness characteristic, *Journal of Sound and Vibration* 301 (301) (2007) 678–689.
[10] A. Carrella, M.J. Brennan, T.P. Waters, V. Lopes Jr., Force and displacement transmissibility of a nonlinear isolator with high-static-low-dynamic-stiffness, *International Journal of Mechanical Sciences* 55 (1) (2012) 22–29.
[11] I. Kovacic, M.J. Brennan, T.P. Waters, A study of a nonlinear vibration isolator with a quasi-zero stiffness characteristic, *Journal of Sound and Vibration* 315 (3) (2008) 700–711.
[12] N. Zhou, K. Liu, A tunable high-static low-dynamic stiffness vibration isolator, *Journal of Sound and Vibration* 329 (9) (2010) 1254–1273.
[13] W.S. Robertson, M.R.F. Kidner, B.S. Cazzolato, A.C. Zander, Theoretical design parameters for a quasi-zero stiffness magnetic spring for vibration isolation, *Journal of Sound and Vibration* 1–2 (2009) 88–103.
[14] R.A. Ibrahim, Recent advances in nonlinear passive vibration isolators, *Journal of Sound and Vibration* 314 (3–5) (2008) 371–452.
[15] T.D. Le, K.K. Ahn, A vibration isolation system in low frequency excitation region using negative stiffness structure for vehicle seat, *Journal of Sound and Vibration* 330 (26) (2011) 6311–6335.
[16] D. Xu, Y. Zhang, J. Zhou, J. Lou, On the analytical and experimental assessment of performance of a quasi-zero-stiffness isolator, *Journal of Vibration and Control* 20 (15) (2014) 2314–2325.
[17] X. Huang, X. Liu, J. Sun, Z. Zhang, H. Hua, Vibration isolation characteristics of a nonlinear isolator using euler buckled beam as negative stiffness corrector: *a theoretical and experimental study*, *Journal of Sound and Vibration* 333 (4) (2014) 1132–1148.
[18] X. Huang, X. Liu, J. Sun, Z. Zhang, H. Hua, Effect of the system imperfections on the dynamic response of a high-static-low-dynamic stiffness vibration isolator, *Nonlinear Dynamics* (2014) 1–11.
[19] X.C. Huang, X.T. Liu, H.X. Hua, Effects of stiffness and load imperfection on the isolation performance of a high-static–low-dynamic-stiffness non-linear isolator under base displacement excitation, *International Journal of Non-Linear Mechanics* 65 (0) (2014) 32–43.
[20] A.D. Shaw, S.A. Neild, D.J. Wagg, Dynamic analysis of high static low dynamic stiffness vibration isolation mounts, *Journal of Sound and Vibration* 332 (6) (2013) 1437–1455, http://dx.doi.org/10.1016/j.jsv.2012.10.036.
[21] D.J. Wagg, S.A. Neild, *Nonlinear Vibration with Control*, Springer, Berlin, Germany, 2009.

[22] S.A. Neild, Approximate methods for analysing nonlinear structures, in: L.N. Virgin, D.J. Wagg (Eds.), *Exploiting Nonlinear Behaviour in Structural Dynamics*, Springer, Berlin, Germany, 53–109.
[23] S.A. Neild, D.J. Wagg, Applying the method of normal forms to second-order nonlinear vibration problems, *Proceedings of the Royal Society A* 467 (2128) (2010) 1141–1163.
[24] Z. Xin, S.A. Neild, D.J. Wagg, The selection of the linearized natural frequency for the second-order normal form method, *ASME* (2011).
[25] Z. Xin, Z. Zuo, H. Feng, D.J. Wagg, S.A. Neild, Higher order accuracy analysis of the second-order normal form method, *Nonlinear Dynamics* 70 (3) (2012) 2175–2185.
[26] K. Worden, G.R. Tomlinson, *Nonlinearity in Structural Dynamics*, Institute of Physics, Bristol, United Kingdom, 2001.
[27] S.A. Neild, D.J. Wagg, A generalized frequency detuning method for multidegree-of-freedom oscillators with nonlinear stiffness, *Nonlinear Dynamics* 73 (1–2) (2013) 649–663.